

Article

The Polar Lipid Fraction E from *Sulfolobus acidocaldarius* Can Be Used as Liposomal Drug Stabilizing Agents to Reduce the Leakage of the Antivascular Drug Combretastatin A4 Disodium Phosphate from Tetraether/Diester Hybrid Archaeosomes

Varsha P. Daswani, Umme Ayesa and Parkson Lee-Gau Chong *

Department of Medical Genetics and Molecular Biochemistry,
The Lewis Katz School of Medicine at Temple University, Philadelphia, PA 19140, USA;
vpd816@gmail.com (V.P.D.); ayesa.u@outlook.com (U.A.)

* Correspondence: pchong02@temple.edu; Tel.: +1-215-707-4182

Abstract: Liposomes have many advantages as therapeutic capsules over free drugs such as small molecule drugs and nucleic acids. Cholesterol is commonly used as a membrane stabilizing agent in liposomal drugs (e.g., mRNA-lipid nanoparticle COVID-19 vaccines). However, due to the vulnerability of cholesterol to oxidation and the etiological role of cholesterol in many disorders, it is desirable to find an alternative means to stabilize liposomal membranes for drug delivery. In this study, we demonstrated that the polar lipid fraction E (PLFE), which contains exclusively bipolar tetraether macrocyclic lipids, isolated from the thermoacidophilic archaeon *S. acidocaldarius* can greatly stabilize the liposomal formulation of the anti-vascular drug, combretastatin A4 disodium phosphate (CA4P). Stability was assessed by determining the leakage rate constant k of entrapped CA4P fluorometrically. We found that, at 37 °C, PLFE decreases the k value monotonically from $1.54 \times 10^{-2} \text{ s}^{-1}$ for 100% 1-palmitoyl-2-oleoyl-glycero-3-phosphocholine (POPC) liposomes to $3.4 \times 10^{-5} \text{ s}^{-1}$ for 100% PLFE archaeosomes, a change of k by two orders of magnitude. The changes in k of CA4P leakage are correlated well with the changes in liposomal CA4P's cytotoxicity against MCF-7 breast cancer cells. We further showed that the reduction in spontaneous leakage of entrapped CA4P by PLFE can be attributed to the increased membrane surface charge and the increased membrane order and packing tightness in liposomes, as reflected by the zeta potential (−6.83 to −41.1 mV from 0 to 100 mol% PLFE) and diphenylhexatriene (DPH) fluorescence polarization (0.13 to 0.4 from 0 to 100 mol% PLFE) measurements. Moreover, we showed that PLFE slows down CA4P leakage more than cholesterol in POPC liposomes. These results together suggest that PLFE lipids can serve as an effective stabilizing agent for liposomal drugs and could potentially be useful for the optimization of liposomal CA4P for cancer treatment.

Keywords: stabilizing agents of liposomal drugs; thermoacidophiles; bipolar tetraether lipids; archaeosomes; membrane stability; zeta potential; membrane packing tightness



Citation: Daswani, V.P.; Ayesa, U.; Chong, P.L.-G. The Polar Lipid Fraction E from *Sulfolobus acidocaldarius* Can Be Used as Liposomal Drug Stabilizing Agents to Reduce the Leakage of the Antivascular Drug Combretastatin A4 Disodium Phosphate from Tetraether/Diester Hybrid Archaeosomes. *Biophysica* **2021**, *1*, 474–486. <https://doi.org/10.3390/biophysica1040034>

Academic Editors: Dirk Schneider and Ayumi Hirano-Iwata

Received: 21 September 2021

Accepted: 6 December 2021

Published: 9 December 2021

Publisher's Note: MDPI stays neutral with regard to jurisdictional claims in published maps and institutional affiliations.



Copyright: © 2021 by the authors. Licensee MDPI, Basel, Switzerland. This article is an open access article distributed under the terms and conditions of the Creative Commons Attribution (CC BY) license (<https://creativecommons.org/licenses/by/4.0/>).

1. Introduction

The advantages of using liposomal drugs as opposed to free drugs are well-documented in the literature [1] which include the ability to selectively deliver liposomes to the desired site in the body, reducing the potential side effects, and increasing the therapeutic efficacy. To date, there are more than 20 liposomal anticancer drugs on the market or under clinical trials [2–5], as well as some vaccines such as for COVID-19, which uses lipid carriers for mRNA delivery [5,6]. Most lipid-based carriers include cholesterol as a major component and a membrane stabilizer [3]. However, the use of cholesterol in drug carriers draws some serious concerns because cholesterol is prone to oxidation which can generate a variety of oxysterols leading to biomedical problems such as strokes, hypertension, and cardiovascular diseases. In addition, cholesterol affects liposome physical properties in a

very complicated way. In a previous study, we showed that the leakage and cytotoxicity of the liposomal anti-vascular drug combretastatin A4 disodium phosphate (CA4P) vary with the cholesterol content in the liposomal membrane in an alternating, rather than a monotonic, manner [7]. At critical cholesterol mole fractions (C_r) (e.g., 20.0, 22.2, 25.0, 33.3, 40.0, and 50.0 mol%) for maximal sterol superlattice formation, CA4P can be released from the liposomes more readily than at non-critical cholesterol mole fractions, probably due to the increased domain boundaries between superlattice and non-superlattice regions, which consequently results in increased cytotoxicity at C_r [7]. Taking into consideration these complexities and complications with cholesterol, a new membrane stabilizer for liposomal drugs is needed.

In the present study, we use liposomal CA4P as a model to address this issue. CA4P is a water-soluble prodrug currently under clinical trials for cancer therapy. After administration, CA4P can be taken up by cells and hydrolyzed by intracellular phosphatases to the pharmaceutically active form CA4 (combretastatin A4) [8]. CA4 tends to accumulate in tumor tissues and bind β -tubulin, hence inhibiting microtubule assembly in blood vessel endothelial cells and generating a massive blood vessel collapse, resulting in nutrient deprivation in the developing tumor and eventually tumor necrosis [9]. CA4P can induce vascular shutdown within tumors at doses less than one-tenth of the maximum tolerated dose [10].

A liposome delivery system for CA4P has previously been developed for animal studies [11]. The system contained unilamellar vesicles composed of hydrogenated soybean phosphatidylcholine (HSPC), cholesterol, distearoyl phosphoethanolamine-polyethylene-glycol-2000 conjugate (DSPE-PEG), and DSPE-PEG-maleimide. DSPE-PEG-maleimide was used to link a functional peptide (anti-E-selectin) to guide the liposomes to the target. The initial concentration of CA4P entrapped inside the liposomes was 40 mM [11], at which J-aggregates of CA4P were formed [12]. Aggregates must dissociate into monomeric CA4P before spontaneous transmembrane diffusion can occur [12]. It was demonstrated that targeting these anti-E-selectin conjugated immunoliposomes (IL) loaded with CA4P to MCa-4 mammary tumors in mice treated with therapeutic doses of ionizing radiation (IR) resulted in a significant delay in tumor growth when compared with other treatment groups such as free CA4P, tumor irradiation alone, liposomal CA4P alone, and empty liposomes [11]. Radiation was used to upregulate the expression of endothelial cell adhesion protein molecules (e.g., E-selectin), which provided a means for targeting drugs to irradiated tissue. While this approach is very promising, the overall efficacy of the liposomal CA4P remains somewhat low. The combination treatment with IR and IL still allowed tumors to increase in size over time, although the rate was reduced significantly [11].

One conceivable method to improve this efficacy problem is to optimize the liposomal CA4P formulations. In the present study, we attempt to stabilize liposomal CA4P by introducing an archaeal tetraether lipid component, namely, the polar lipid fraction E (PLFE) isolated from the thermoacidophilic archaeon *Sulfolobus acidocaldarius* [13,14]. PLFE is a mixture of GDNT (glycerol dialkylcalditol tetraether) and GDGT (glycerol dialkylglycerol tetraether) (Figure S1) [13,14]. The GDNT component (~90% of total PLFE) contains phospho-*myo*-inositol on the glycerol end and β -glucose on the calditol end, whereas the GDGT component (~10% of total PLFE) has phospho-*myo*-inositol attached to one glycerol and β -D-galactosyl-D-glucose to the other glycerol skeleton (Figure S1). The nonpolar regions of these lipids consist of a pair of 40-carbon biphytanyl chains, each of which is made of isoprene units and contains up to four cyclopentane rings [15]. The number of cyclopentane rings increases with increasing growth temperature [15–18] and with increasing pH in growth media [19]. The dibiphytanyl chains are linked to either two glycerol (in the case of GDGT), or one glycerol and one calditol (in the case of GDNT) moieties via tetraether bonds, forming a macrocyclic molecule (Figure S1).

PLFE lipids are tetraethers, which are chemically more stable than diester lipids. Ester-linked phospholipids may be hydrolyzed by water during long-term storage, whereas the tetraether-linked PLFE is not prone to hydrolysis. In addition, PLFE lipids do not have

C=C double bonds in the hydrocarbon chains; thus, PLFE lipids are also stable against auto-oxidation. These properties suggested that using PLFE to make model membranes (such as liposomes and planar membranes) would make the membranes more chemically stable compared to those made of diester lipids.

Indeed, previous studies have shown that PLFE lipids can form extraordinarily stable unilamellar (~60–800 nm in diameter), multilamellar, and giant unilamellar (~10–150 μm) vesicles [13,20] as well as free-standing [21,22] and solid-supported [23] planar membranes. In this study, PLFE-containing liposomes are referred to as archaeosomes. PLFE lipids in the archaeosomal membranes span the entire lamellar structure, forming a monomolecular thick membrane [24], which contrasts to the bilayer structure formed by diester or diether lipids. Compared to liposomes made of diester or diether lipids, PLFE archaeosomes exhibit unusual membrane physical properties (reviewed in [25–27]). PLFE liposomes exhibit low proton/dye permeability, high stability against autoclaving and fusogenic compounds, tight and rigid membrane packing, low enthalpy and volume changes associated with the phase transitions, low isothermal/adiabatic compressibility, and low relative volume fluctuations. The remarkable chemical and physical stability of PLFE archaeosomes, along with their low cytotoxicity in animals [28–30], makes them appealing for biomedical applications such as the targeted delivery of therapeutic agents.

In the present study, we examined the ability of PLFE lipids to retain entrapped CA4P drug molecules inside archaeosomes made of PLFE and 1-palmitoyl-2-oleoyl-glycerol-3-phosphocholine (POPC). We chose to study this PLFE/POPC tetraether/diester hybrid archaeosome system because the physical properties of POPC and PLFE liposomes are well documented in the literature (e.g., [25,31,32]) and because the leakage and cytotoxicity of CA4P in POPC liposomes with varying amounts of cholesterol have previously been studied [7], which permits the comparison of the stabilizing effect of PLFE with that of cholesterol on liposomal CA4P. Membrane stability can be assessed by the measurements of the rate constant of spontaneous leakage of the entrapped drug molecules [33]. In this study, we measured CA4P leakage from PLFE/POPC archaeosomes using CA4P's intrinsic fluorescence [7].

The obtained results indicate that an increase in PLFE content decreases CA4P spontaneous leakage significantly, with PLFE liposomes having a leakage rate constant at least two orders of magnitude lower than POPC liposomes, and that the changes in leakage rate constant are correlated with the changes in liposomal CA4P cytotoxicity against MCF-7 breast cancer cells. Our data also indicate that the reduction in spontaneous leakage of entrapped CA4P by PLFE can be attributed to the increased membrane surface charge and the increased membrane order in liposomes, as reflected by the zeta potential and 1,6-diphenyl-1,3,5-hexatriene (DPH) fluorescence polarization values. These results may pave the way of using archaeosomal CA4P for cancer treatment.

2. Materials and Methods

2.1. Archaea Cells and PLFE Lipids

S. acidocaldarius cells (ATCC #49426, Rockville, MD, USA) were grown aerobically and heterotrophically at ~75–80 °C and pH 2.5–3.0. The polar lipid fraction E (PLFE) was isolated from *S. acidocaldarius* dry cells as previously described [13,14]. POPC was purchased from Avanti Polar Lipids (Alabaster, AL, USA). The concentrations of PLFE and POPC in stock solutions were determined based on the dry weight and the phosphate assay [34], respectively.

2.2. Particle Size, Size Distribution, and Zeta Potential

The hydrodynamic diameters of vesicles were measured at 25 °C by photon correlation spectroscopy using a Malvern Zetasizer 1000 HAS spectrometer (Malvern Panalytical Ltd, Malvern, UK). The light source was a 10 mW He-Ne laser (633 nm) and the scattered light was measured at 90° to the incident beam using an avalanche photodiode detector. The data were analyzed using the Contin algorithm (provided by Malvern Instruments), which

calculates the average size and polydispersity. The former is the average hydrodynamic diameter of the vesicles whereas the latter is a measure of the width of the vesicle size distribution. Liposome zeta potential was determined on a Malvern Zetasizer Nano ZS instrument (Malvern Panalytical Ltd, Malvern, UK), which uses a combination of laser Doppler velocimetry and phase analysis light scattering to measure particle electrophoretic mobility (U_E). U_E is then converted to zeta potential by the Henry equation: $U_E = 2 \epsilon z f(\kappa a)/3\eta$, where z = zeta potential, ϵ = dielectric constant, η = viscosity, and Henry function $f(\kappa a) = 1.5$. Zeta potential data was gathered in subsets of 100 runs and analyzed on the Malvern Zetasizer and Origin software.

2.3. Liposome Preparation

Appropriate proportions were taken from PLFE (in chloroform/methanol/water, 66/31/7, *v/v/v*) and POPC (in chloroform) stock solutions and combined in round bottom Pyrex tubes to make PLFE/POPC liposomes with desired molar ratios. The solvents were evaporated to dryness by first flushing with nitrogen gas and then by placing it under a high vacuum overnight. The dry lipids were suspended in 50 mM Tris buffer (pH 7.2) containing 10 mM EDTA, with or without (for the cytotoxicity study) 0.02% NaN_3 . Multilamellar vesicles were formed via vortexing at 65 °C for 2–3 min. The multilamellar vesicles were extruded (Lipex Biomembranes, Vancouver, Canada) 10 times through two stacked Nucleopore polycarbonate membranes (membrane pore size: 50, 100, or 200 nm) under N_2 gas pressure to make unilamellar vesicles [35,36]. Vesicles were then flushed with argon and stored in a low vacuum chamber to prevent lipid oxidation. The extruded vesicles had a polydispersity of < 0.17, indicative of homogenous size distribution.

2.4. DPH Fluorescence Polarization Measurements

Unilamellar vesicles in 50 mM Tris buffer (pH 7.2) containing 10 mM EDTA and 0.02% NaN_3 were labeled with 3.3 μL of 30 μM DPH (Molecular Probes, Eugene, OR, USA) in methanol. The probe-to-lipid molar ratio was $\sim 1/400$. After 1 h incubation at 50 °C with stirring, DPH in liposomes was excited at 350 nm and the emission was observed at 428 nm at 25 °C via a monochromator on an ISS K2 fluorometer (Champaign, IL, USA). The background intensity was subtracted from sample readings. Emission polarization of DPH in liposomes was calculated as described [37].

2.5. Entrapment of CA4P in Archaeosomes

CA4P (synthesized as described in [38]) was photo-activated to *trans*-CA4P [39] using the procedures given in [12]. *Trans*-CA4P was used exclusively for the experimental work described in this paper. For simplicity, the subsequent use of the term CA4P is referring to *trans*-CA4P. In the leakage and cytotoxicity studies, the buffer that was used to make liposomes contained 5 mM CA4P. Thus, the initial CA4P concentration entrapped in the interior compartment of the liposomes was ~ 5 mM. At this concentration, CA4P fluorescence is self-quenched [12].

2.6. Separation of Free CA4P from Archaeosomal CA4P

Immediately before the cytotoxicity assay or the CA4P leakage experiment, free CA4P was removed by a Sephadex G-50 gel filtration column. The column was loaded with liposomal CA4P and eluted with 50 mM Tris buffer (pH 7.2) containing 10 mM EDTA. The elution profile was determined using light scattering ($\lambda_{\text{ex}} = 500$ nm and $\lambda_{\text{em}} = 505$ nm) and CA4P fluorescence intensity ($\lambda_{\text{ex}} = 328$ nm and $\lambda_{\text{em}} = 400$ nm) measured on an ISS K2 fluorometer (Champaign, IL). The fractions containing liposomes with entrapped CA4P were pooled. The amount of CA4P in liposomes was determined by first extracting the pooled fractions with 2 mL of choloform:methanol (2:1, *v/v*) [7]. The entrapped CA4P (which is water-soluble) was released from liposomes and partitioned into the aqueous phase. The amount of CA4P entrapped in the liposomes was determined by measuring the absorbance at 300 nm of the aqueous phase on a Perkin-Elmer lambda-25

spectrophotometer and using the extinction coefficient of CA4P equal to $5640 \text{ M}^{-1}\text{cm}^{-1}$ ($\lambda_{\text{abs}} = 328 \text{ nm}$ measured in methanol) [7].

2.7. Drug Leakage Assay

Leakage of entrapped CA4P from archaeosomes was monitored by measuring the enhancement of CA4P fluorescence intensity due to the relief of self-quenching [7,12]. Specifically, 200 μL of liposomal CA4P dispersions containing 0.5 nmol of CA4P collected from Sephadex G-50 (described above) was pipetted into a cuvette with 2 mL of 50 mM Tris buffer (pH 7.2) containing 10mM EDTA and 0.02% NaN_3 . The lipid concentration in the cuvette was $\sim 12 \mu\text{M}$ [7]. The liposome dispersions under mild magnetic stirring in the cuvette were excited at 328 nm, and the fluorescence intensity at 400 nm (F_t) was recorded as a function of time on the ISS K2 fluorometer. At the end of each leakage experiment, the sample was mixed with the detergent n-tetradecyl- β -D-maltoside (TDM) (Anatrace, Maumee, OH) and the final TDM concentration in the cuvette was 100 μM . TDM was mixed with liposomes for 20 min to release all the entrapped CA4P, which provides the maximal fluorescence intensity (F_{max}) values. The equation for the first-order kinetics $F = A + B(1 - e^{-kt})$, where k is the rate constant of leakage, t is time, and A and B are constants, was used to fit the normalized fluorescence intensity $F (=F_t/F_{\text{max}})$ [7,12]. For each membrane system examined, the leakage assay was repeated three times.

2.8. MCF-7 Cell Line

Human MCF-7 breast cancer cells (ATCC) were grown at 37°C with 5% CO_2 atmosphere using a complete growth medium composed of Dulbecco's modification of Eagle's medium (DMEM $1\times$, with 4.5g/L glucose, L-glutamine, and sodium pyruvate) supplemented with 10% fetal bovine serum and 1% penicillin/streptomycin. When $\sim 80\%$ confluency was reached, cells were detached using 0.25% trypsin-EDTA, rinsed with phosphate-buffered saline, and collected after centrifugation at $2000\times g$ for 5 min at 25°C .

2.9. Cytotoxicity Assay

MCF-7 cells were resuspended into a complete growth medium, plated into a 96-well microplate ($\sim 10,000$ cells per well), and maintained in a serum-containing medium for >12 h until the cells adhered to the wall of the microplate wells. After the MCF-7 cells were treated with liposomal CA4P for the desired time period at 37°C , the dead cells (floating in the growth medium) were removed. The cell proliferation assay was performed to determine the number of cells remaining alive (defined as those still attached to the well). The assay was performed at room temperature ($\sim 25^\circ\text{C}$) using the CyQuant kit (Invitrogen, Carlsbad, CA, USA) according to the manufacturer's instructions. Fluorescence intensities at 530 nm were measured on a Spectra Max M5 microplate reader (Molecular Devices, Sunnyvale, CA, USA) with excitation at 485 nm. A standard curve was constructed for each sample set using known amounts of MCF-7 cells counted with a hemacytometer so that the fluorescence intensities could be converted to the cell numbers. Typically, 0.5 nmole of CA4P in liposomes was added to each of the 96-wells in the microplate, which had $\sim 10,000$ cells per well at time zero.

2.10. Statistical Analysis

Data were expressed as the mean \pm standard deviation. To test if there was a statistically significant difference between certain data points, a paired Student's t -test (two-tailed) was performed, and a p -value was calculated.

3. Results and Discussion

3.1. CA4P Leakage

We have determined the rate constant of CA4P leakage from the interior of the PLFE/POPC archaeosomes to the bulk aqueous phase outside the vesicles using the method previously described [7,12]. The results are presented in Figure 1A. The rate

constant k decreases steadily with increasing PLFE content. Compared to 100 mol% POPC liposomes, 100 mol% PLFE archaeosomes have a leakage rate constant at least two orders of magnitude lower. For a given PLFE-to-POPC molar ratio, the rate constant at 37 °C is slightly higher than that at 25 °C ($p < 0.05$), except for 100% PLFE. It is important to note that, in the case of CA4P leakage from cholesterol/POPC liposomes [7], the leakage rate does not change with cholesterol mole fraction in a monotonic manner; instead, the leakage rate of CA4P changes with cholesterol in an alternating manner following the principle of sterol superlattice formation [7]. In the case of using cholesterol as the stabilizing agent for liposomal CA4P, the overall leakage rate can be changed ~ 1.6 times from 18 to 55 mol% cholesterol [7], which is comparable to the leakage rate constant change from 18 to 55 mol% PLFE (Figure 1A). However, when PLFE is used as the stabilizing agent, the amount of PLFE can go up to 100 mol% whereas when cholesterol is used as the stabilizing agent, the cholesterol content in POPC cannot go beyond 66.7 mol%, the maximal solubility of cholesterol in phosphatidylcholine bilayers [40].

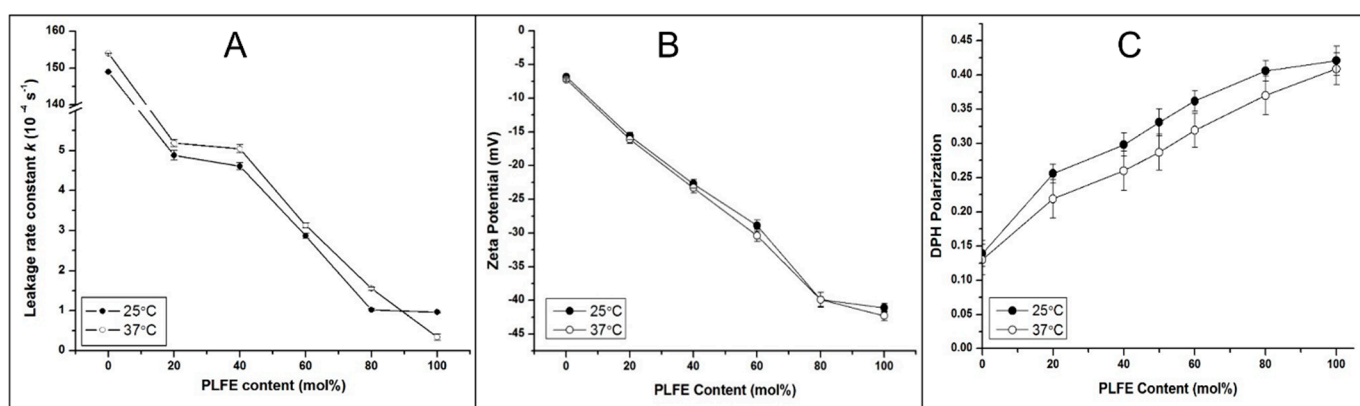


Figure 1. Effects of PLFE content in PLFE/POPC unilamellar vesicles (~ 131 – 200 nm in diameter) on (A) CA4P leakage rate constant k , (B) zeta potential, and (C) the steady-state polarization of DPH fluorescence, at 25 °C and 37 °C. Vesicles were dispersed in 50 mM Tris (pH 7.2) containing 10 mM EDTA and 0.02% NaN_3 . The error bars were the standard deviations of the measurements from three different samples.

3.2. Zeta Potential

For the entrapped drug molecule to leak out of the vesicles, it must overcome three energy barriers: the polar headgroup region facing the interior aqueous compartment of the liposome, the hydrophobic core, and the polar headgroup region facing the exterior of the liposome. It has been suggested that, due to the presence of sugar and phosphate moieties on PLFE (Figure S1), the polar headgroup regions of 100% PLFE archaeosomes have a strong hydrogen bond network [41–43]. As PLFE is negatively charged at neutral pH, increasing PLFE content in the mixture of PLFE and POPC should increase the surface charge and the surface potential as well as the hydrogen bond network strength, which could contribute to the decrease in k with increasing PLFE content (Figure 1A).

To test the proposition that the surface potential of liposomes can be altered by PLFE, we measured the zeta potential of PLFE/POPC archaeosomes with varying molar ratios at 25 and 37 °C (Figure 1B). The zeta potential is the potential at the hydrodynamic plane of shear, which is not the same as the membrane surface potential [43], however, it reflects the particle's surface charge. In the case of archaeosomes containing negatively charged PLFE lipids, the zeta potential is expected to be less negative than the surface potential [44,45]. As shown in Figure 1B, the zeta potential of PLFE/POPC archaeosomes changed significantly with PLFE content, for example, from -6.83 ± 0.31 mV for 100% POPC to -41.1 ± 0.64 mV for 100% PLFE at 25 °C. These two zeta potential values are consistent with those previously reported for 100% POPC and 100% PLFE [46,47]. Between 0–100 mol% PLFE in POPC, the zeta potential decreases with increasing PLFE content in a monotonic manner (Figure 1B). This trend is different from that found in PLFE/1,2-dipalmitoyl-glycerol-3-phosphocholine

(DPPC) archaeosomes at 25 °C, where zeta potential decreases with increasing PLFE content till 60 mol%, after which zeta potential increases with increasing PLFE content [48]. PLFE lipids are macrocyclic, asymmetric molecules, with one polar end negatively charged at neutral pH and the other polar end un-charged. The zeta potential of PLFE-containing archaeosomes depends on the transmembrane orientation of PLFE lipids [48,49]. It may be implied from our data that fluid state POPC (Figure 1B) and gel state DPPC (Figure 1 in [48]) have different influences on PLFE transmembrane orientation, especially at high PLFE content. In addition, Figure 1B shows that PLFE/POPC liposomes at high PLFE content (i.e., >60 mol%) would be highly stable against aggregation or coalescence due to strong negative-negative charge repulsions between vesicles. Traditionally, particles with zeta potential values more negative than -30 mV or more positive than $+30$ mV are regarded as being of high stability during long-term storage [50].

3.3. Effect of PLFE Content on Archaeosomal Membrane Packing in the Hydrophobic Core

To test whether the decreased leakage rate constant with increasing PLFE (Figure 1A) is partly due to the increased packing tightness in the hydrocarbon core, we measured the steady-state polarization of DPH fluorescence in PLFE/POPC archaeosomes as a function of PLFE content. The DPH polarization value of 100% POPC liposomes is 0.14 at 25 °C (Figure 1C), which agrees well with that previously reported [51]. The steady-state polarization of DPH fluorescence reflects mainly the molecular order in the hydrocarbon core of liposomal membranes, especially when the DPH polarization value is > 0.22 and the fundamental polarization of DPH (i.e., the polarization when the probe does not rotate at all) is close to the theoretical maximum value 0.50 [52]. It is evident from Figure 1C that in the mixture of PLFE/POPC, all the DPH polarization values, except for those at 0 mol% PLFE, are greater than 0.22. Thus, the DPH polarization data can be taken to indicate that the membrane order increases steadily with increasing PLFE content at 25 and 37 °C.

From Figure 1B,C it can be concluded that an increase in PLFE content in PLFE/POPC archaeosomes increases zeta potential on the particle surface and increases packing tightness in the liposomal membrane, both of which could in turn lead to a steady decrease in leakage rate constant with increasing PLFE content (Figure 1A).

We have also measured the CA4P leakage rate constant in 20 mol% cholesterol/80 mol% POPC versus 20 mol% PLFE/80 mol% POPC (Figure 2). It is found that the presence of PLFE in the POPC membrane system slows down CA4P leakage more than the presence of cholesterol in POPC ($p < 0.05$).

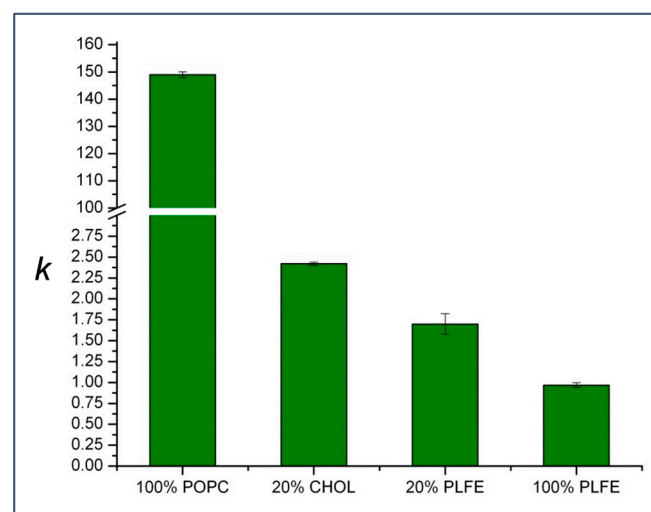


Figure 2. The CA4P leakage rate constant k (10^{-4} s^{-1}) from 100% POPC liposomes, 20 mol% cholesterol/80 mol% POPC liposomes, 20 mol% PLFE/80 mol% POPC archaeosomes, and 100% PLFE archaeosomes. Size = ~ 170 nm; Temperature = 25 °C.

3.4. Effect of PLFE Content on Cytotoxicity of Archaeosomal CA4P against MCF-7 Breast Cancer Cells

We used MCF-7 human breast cancer cells as a model to test the cytotoxicity of PLFE-based archaeosomal CA4P. The number of surviving cells (Figure 3A) was determined by the CyQuant assay kit. Each time trace in Figure 3A can be fitted into an exponential decay function to obtain the apparent rate constant of toxicity change k' . When the drug leakage rate constant k is decreased, the rate constant of cell death k' is decreased accordingly. The changes in k of drug leakage (Figure 1A) are correlated well with the changes in the rate constant of liposomal CA4P's cytotoxicity against MCF-7 breast cancer cells, with a correlation coefficient of 0.86 (Figure 3B).

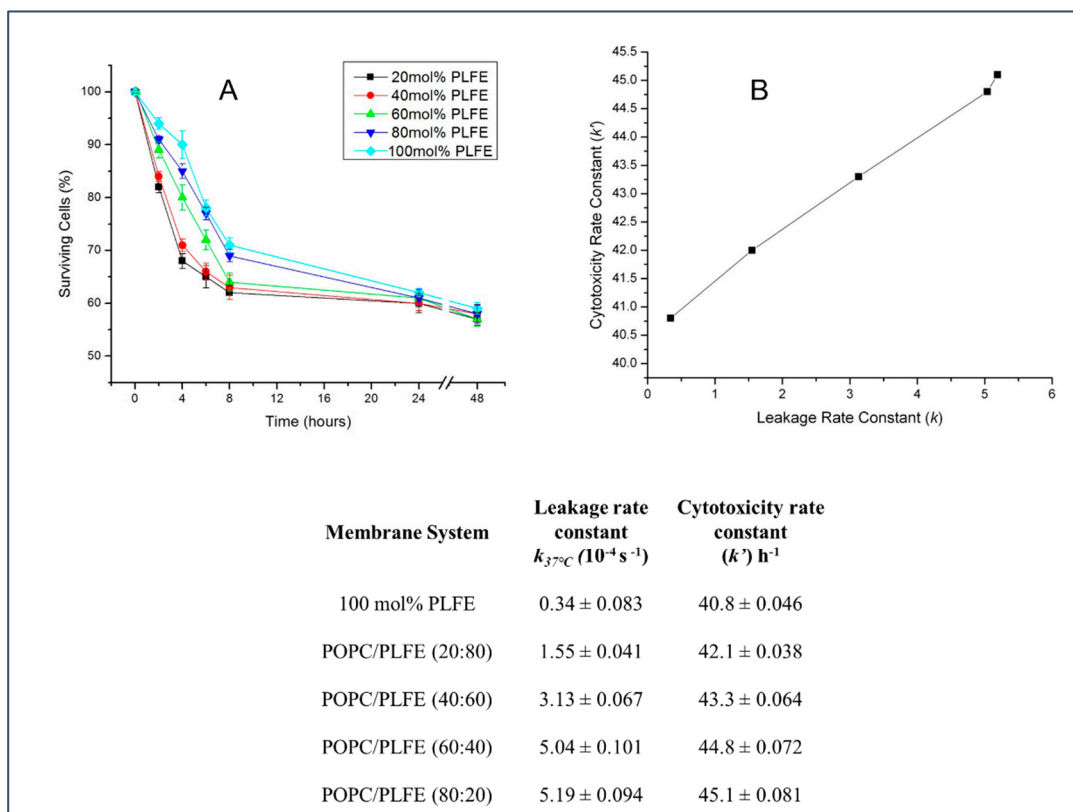


Figure 3. (A) The time course of the percent of MCF-7 breast cancer cells remaining alive after treatment with PLFE/POPC archaeosomal CA4P with varying PLFE mole fractions. (B) Correlation between the CA4P leakage rate constant k and the cytotoxicity rate constant k' , with all the rate constants listed.

3.5. Effect of Archaeosome Size on Drug Leakage and Cytotoxicity

Figure 4A shows the effect of vesicle size on the spontaneous leakage of entrapped CA4P from 100% PLFE archaeosomes. The leakage rate constant increased slightly when the vesicle size was varied from 256 to 102 nm (Figure 4A, $p < 0.05$). However, the rate constant increased much more significantly (~1.8 times) when the vesicle size was further reduced to ~60 nm. In terms of achieving a low spontaneous leakage rate, PLFE liposomes with 256 nm in diameter were the most desirable among all the formulations examined. This trending is different from that of proton permeation across PLFE archaeosomal membranes. In a previous study, we have shown that small PLFE archaeosomes (~60 nm in diameter) exhibited a lower proton permeability than larger PLFE archaeosomes (~240 nm in diameter) [46], which was explained as the result of curvature-induced changes in PLFE transmembrane asymmetry. One possible explanation for this discrepancy is that since CA4P carries a phosphate moiety and three methoxy groups, CA4P may interact with PLFE polar headgroups via hydrogen bonding or other non-covalent interactions, while being water-soluble and entrapped in the interior aqueous compartment of the archaeosomes.

Such interactions may prevent PLFE from undergoing changes in transmembrane asymmetry when the membrane curvature is increased (i.e., when the particle size is reduced).

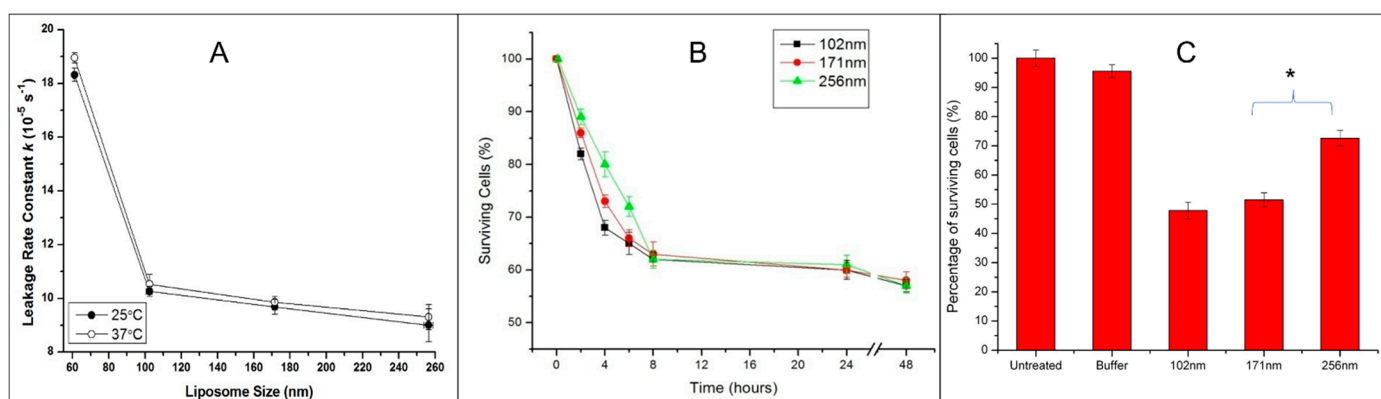


Figure 4. Effect of particle diameter in 100% PLFE archaeosomes on (A) CA4P leakage rate constant at 25 and 37 °C, (B) archaeosomal CA4P-induced cytotoxicity in MCF-7 cells at 37 °C, and (C) the cytotoxicity of 100% PLFE archaeosomal CA4P after incubation with MCF-7 cells at 37 °C for 5 h (*: $p < 0.05$).

We have also examined the effect of vesicle size on the cytotoxicity of archaeosomal CA4P against MCF-7 cells (Figure 4B,C). Over the 48-h incubation time, ~58% of cells survived; however, the initial rate of cytotoxicity varied with particle size (Figure 4B). PLFE archaeosomes with a diameter of 256 nm gave a lower rate of cell death compared to those at 102 and 171 nm in diameter. This result is particularly obvious when the cytotoxicity data obtained after 5 h of incubation are plotted (Figure 4C). The cytotoxicity data is correlated well with the CA4P spontaneous leakage rate constant, giving a correlation coefficient of 0.91.

4. Conclusions

Our present work used the anticancer drug CA4P and the bipolar tetraether lipids PLFE to illustrate from the biophysical point of view that bipolar tetraether archaeal lipids can serve as an effective (if not better) membrane stabilizing agent in liposomal drug formulations.

Our data show that PLFE tetraether lipids can stabilize liposomes against drug leakage, liposome coalescence, and membrane disruption. As a stabilizing agent for liposomal drugs, PLFE tetraether lipids have advantages over cholesterol. First, the amount of cholesterol in a liposome is restricted by the cholesterol solubility limit. For phosphatidylcholine liposomes, when the cholesterol content is greater than 66.7 mol%, cholesterol will precipitate out forming micro-crystals [40]. In contrast, the PLFE content in liposomes has no limit. Liposomes can be formed with 0–100% PLFE. Second, the DPH polarization value (inferentially, membrane order) changes from 0.14 to 0.31 when the cholesterol content in POPC liposomes is changed from 0 to 50 mol% [51]. In comparison, the DPH polarization changes from 0.14 to 0.41 when the PLFE content in POPC is varied from 0 to 100 mol% (Figure 1C). Like cholesterol, PLFE increases DPH polarization and thus membrane order. However, the magnitude of the DPH polarization that can be changed by PLFE in PLFE/POPC hybrid systems is greater than that changed by cholesterol in cholesterol/POPC systems. Therefore, in terms of tightening membrane packing in the hydrophobic core, PLFE can provide a wider range of alterations than cholesterol. In addition, at the same mole fraction in POPC vesicles, PLFE slows down CA4P leakage more than cholesterol (Figure 2). Third, although cholesterol can tighten membrane packing, cholesterol does not change vesicle zeta potential and thus does not increase liposome stability against colloidal aggregation/coalescence. In sharp contrast, the zeta potential of PLFE/POPC liposomes can be changed from slightly negative to much more negative (e.g., < -30 mV) when PLFE content is increased from 0 mol% to >60 mol% (Figure 1B).

When the zeta potential becomes < -30 mV, the colloidal particles are usually considered as stable against particle aggregation and coalescence during long-term storage. Finally, it is important to note that PLFE archaeal lipids, unlike cholesterol, are chemically inert and not linked to any human disorders.

CA4P is a promising anti-vascular drug; however, previous studies of liposomal CA4P used mainly conventional diester lipids in the CA4P liposomal formulations [7,11,53]. In 2015, our group reported the first study of archaeosomal CA4P [12] and showed that the leakage of *trans*-CA4P from PLFE archaeosomes follows the first-order kinetics and that the initial CA4P concentration entrapped inside the vesicles should be ≥ 5 mM to sustain a slow and steady drug release due to the formation of CA4P J-aggregates and their slow conversion to monomeric CA4P [12]. In the present study, we found that an increase in PLFE mole fraction caused a significant decrease in the leakage rate constant of *trans*-CA4P from PLFE/POPC liposomes, which can be attributed to the marked increase in surface potential and membrane order. This result implies that, when PLFE-based archaeosomal CA4P is administered in vivo, CA4P can be retained inside the archaeosomes for a longer time, and consequently more CA4P molecules could reach the target than just using conventional diester liposomal CA4P. This proposition will be tested in animal studies in the near future and will advance the research on the use of archaeosomal drugs for therapy in general [54–61].

Supplementary Materials: The following are available online at <https://www.mdpi.com/article/10.3390/biophysica1040034/s1>, Figure S1: Illustration of the molecular structures of PLFE.

Author Contributions: Conceptualization, P.L.-G.C.; methodology, V.P.D. and U.A.; formal analysis, V.P.D. and U.A.; investigation, V.P.D. and U.A.; resources, V.P.D., U.A., and P.L.-G.C.; data curation, V.P.D. and U.A.; writing original draft preparation, V.P.D. and P.L.-G.C.; writing—review and editing, V.P.D., U.A., and P.L.-G.C.; supervision, P.L.-G.C.; project administration, P.L.-G.C.; All authors have read and agreed to the published version of the manuscript.

Funding: This work was supported in part by NSF grant DMR1105277.

Data Availability Statement: Data are contained within the article.

Acknowledgments: The authors thank Mohammad Kiani for providing CA4P and Yuri Persidsky for the use of the Spectra Max M5 microplate reader.

Conflicts of Interest: The authors declare no conflict of interest.

Abbreviations

CA4, combretastatin A4; CA4P, combretastatin A4 disodium phosphate; DPH, 1,6-diphenyl-1,3,5-hexatriene; GDNT, glycerol dialkylcalditol tetraether; GDGT, glycerol dialkylglycerol tetraether; PLFE, polar lipid fraction E; POPC, 1-palmitoyl-2-oleoyl-glycerol-3-phosphocholine-; TDM, *n*-tetradecyl- β -D-maltoside.

References

1. Allen, T.M.; Cullis, P.R. Liposomal drug delivery systems: From concept to clinical applications. *Adv. Drug Deliv. Rev.* **2013**, *65*, 36–48. [[CrossRef](#)] [[PubMed](#)]
2. Olusanya, T.O.B.; Ahmad, R.R.H.; Ibegbu, D.M.; Smith, J.R.; Elkordy, A.A. Liposomal drug delivery systems and anticancer drugs. *Molecules* **2018**, *23*, 907. [[CrossRef](#)] [[PubMed](#)]
3. Immordino, M.L.; Dosio, F.; Cattel, L. Stealth liposomes: Review of the basic science, rationale, and clinical applications, existing and potential. *Int. J. Nanomed.* **2006**, *1*, 297–315.
4. Chang, H.; Yeh, M. Clinical development of liposome-based drugs: Formulation, characterization and therapeutic efficacy. *Int. J. Nanomed.* **2012**, *7*, 49–60.
5. Anselmo, A.C.; Mitragotri, S. Nanoparticles in the clinic: An update post COVID-19 vaccines. *Bioeng. Transl. Med.* **2021**, *6*, e10246. [[CrossRef](#)] [[PubMed](#)]
6. Schoenmaker, L.; Witzigmann, D.; Kulkarni, J.A.; Verbeke, R.; Kersten, G.; Jiskoot, W.; Crommelin, D.J.A. mRNA-lipid nanoparticle COVID-19 vaccines: Structure and stability. *Int. J. Pharm.* **2021**, *601*, 120586. [[CrossRef](#)]

7. Venegas, B.; Zhu, W.; Haloupek, N.B.; Lee, J.; Zellhart, E.; Sugar, I.P.; Kiani, M.; Chong, P.L.-G. Cholesterol superlattice modulates combretastatin A4 disodium phosphate (CA4P) release from liposomes and CA4P cytotoxicity on mammary cancer cells. *Biophys. J.* **2012**, *102*, 2086–2094. [[CrossRef](#)]
8. Young, S.L.; Chaplin, D.J. Combretastatin A4 phosphate: Background and current clinical status. *Expert Opin. Investig. Drugs* **2004**, *13*, 1171–1182. [[CrossRef](#)]
9. Dong, D.; Ko, B.; Baumeister, P.; Swenson, S.; Costa, F.; Markland, F.; Stiles, C.; Patterson, J.B.; Bates, S.E.; Lee, A.S. Vascular targeting and antiangiogenesis agents induce drug resistance effector GRP78 within the tumor microenvironment. *Cancer Res.* **2005**, *65*, 5785–5791. [[CrossRef](#)]
10. Dark, G.G.; Hill, S.A.; Prise, V.E.; Tozer, G.M.; Pettit, G.R.; Chaplin, D.J. Combretastatin A-4, an agent that displays potent and selective toxicity toward tumor vasculature. *Cancer Res.* **1997**, *57*, 1829–1834.
11. Pattillo, C.B.; Venegas, B.; Donelson, F.J.; Del Valle, L.; Knight, L.; Chong, P.L.-G.; Kiani, M.F. Radiation-guided targeting of combretastatin encapsulated immunoliposomes to mammary tumors. *Pharm. Res.* **2009**, *26*, 1093–1100. [[CrossRef](#)]
12. Daswani, V.P.; Ayesa, U.; Venegas, B.; Chong, P.L.-G. Concentration-induced J-aggregate formation causes a biphasic change in the release of *trans*-combretastatin A4 disodium phosphate from archaeosomes and the subsequent cytotoxicity on mammary cancer cells. *Mol. Pharm.* **2015**, *12*, 3724–3734. [[CrossRef](#)] [[PubMed](#)]
13. Lo, S.L.; Montague, C.E.; Chang, E.L. Purification of glycerol dialkyl nonitol tetraether from *Sulfolobus acidocaldarius*. *J. Lipid Res.* **1989**, *30*, 944–949. [[CrossRef](#)]
14. Chang, E.L.; Lo, S.L. Extraction and purification of tetraether lipids from *Sulfolobus acidocaldarius*. In *Protocols for Archaeobacterial Research*; Fleischmann, E.M., Place, A.R., Robb, R.T., Schreier, H.J., Eds.; Maryland Biotechnology Institute: Baltimore, MD, USA, 1991; pp. 2.3.1–2.3.14.
15. De Rosa, M.; Gambacorta, A.; Nicolaus, B.; Chappe, B.; Albrecht, P. Isoprenoid ethers: Backbone of complex lipids of the archaeobacterium *Sulfolobus solfataricus*. *Biochim. Biophys. Acta* **1983**, *753*, 249–256. [[CrossRef](#)]
16. De Rosa, M.; Esposito, E.; Gambacorta, A.; Nicholaus, B.; Bu'lock, J.D. Effects of temperature on ether lipid composition of *Caldariella acidophila*. *Phytochemistry* **1980**, *19*, 827–831. [[CrossRef](#)]
17. Yang, L.L.; Haug, A. Structure of membrane lipids and physico-biochemical properties of the plasma membrane from *Thermoplasma acidophilum*, adapted to growth at 37 °C. *Biochim. Biophys. Acta* **1979**, *573*, 308–320. [[CrossRef](#)]
18. Uda, I.; Sugai, A.; Itoh, Y.H.; Itoh, T. Variation in molecular species of polar lipids from *Thermoplasma acidophilum* depends on growth temperature. *Lipids* **2001**, *36*, 103–105. [[CrossRef](#)] [[PubMed](#)]
19. Shimada, H.; Nemoto, N.; Shida, Y.; Oshima, T.; Yamagishi, A. Effects of pH and temperature on the composition of polar lipids in *Thermoplasma acidophilum* HO-62. *J. Bacteriol.* **2008**, *190*, 5404–5411. [[CrossRef](#)] [[PubMed](#)]
20. Bagatolli, L.A.; Gratton, E.; Khan, T.K.; Chong, P.L.-G. Two-photon fluorescence microscopy studies of bipolar tetraether giant liposomes from thermoacidophilic archaeobacteria *Sulfolobus acidocaldarius*. *Biophys. J.* **2000**, *79*, 416–425. [[CrossRef](#)]
21. Ren, X.; Liu, K.; Zhang, Q.; Noh, H.M.; Kumbur, E.C.; Yuan, W.W.; Zhou, J.G.; Chong, P.L.-G. Design, fabrication and characterization of archaeal tetraether free-standing planar membranes in a PDMS- and PCB-based fluidic platform. *ACS Appl. Mater. Interfaces* **2014**, *6*, 12618–12628. [[CrossRef](#)]
22. Ren, X.; Kumbur, E.C.; Zhou, J.G.; Noh, H.M.; Chong, P.L.-G. Stability of free-standing tetraether planar membranes in microchips. *J. Membr. Sci.* **2017**, *540*, 27–34. [[CrossRef](#)]
23. Jeworrek, C.; Evers, F.; Erlikamp, M.; Grobelny, S.; Tolan, M.; Chong, P.L.-G.; Winter, R. Structure and phase behavior of archaeal lipid monolayers. *Langmuir* **2011**, *27*, 13113–13121. [[CrossRef](#)] [[PubMed](#)]
24. Elferink, M.G.; de Wit, J.G.; Demel, R.; Driessen, A.J.; Konings, W.N. Functional reconstitution of membrane proteins in monolayer liposomes from bipolar lipids of *Sulfolobus acidocaldarius*. *J. Biol. Chem.* **1992**, *267*, 1375–1381. [[CrossRef](#)]
25. Chong, P.L.-G. Archaeobacterial bipolar tetraether lipids: Physico-chemical and membrane properties. *Chem. Phys. Lipids* **2010**, *163*, 253–265. [[CrossRef](#)]
26. Chong, P.L.-G.; Ayesa, U.; Daswani, V.P.; Hur, E.C. On physical properties of tetraether lipid membranes: Effects of cyclopentane rings. *Archaea* **2012**, *2012*, 138439. [[CrossRef](#)] [[PubMed](#)]
27. Chong, P.L.-G.; Bonanno, A.; Ayesa, U. Dynamics and organization of archaeal tetraether lipid membranes. In *Membrane Organization and Dynamics, Springer Series in Biophysics*; Chattopadhyay, A., Ed.; Springer International Publishing: Cham, Switzerland, 2017; pp. 11–30.
28. Freisleben, H.-J.; Bormann, J.; Litzinger, D.C.; Lehr, F.; Rudolph, P.; Schatton, M.; Huang, L. Toxicity and biodistribution of liposomes of the main phospholipid from the archaeobacterium *Thermoplasma acidophilum*. *J. Liposome Res.* **1995**, *5*, 215–223. [[CrossRef](#)]
29. Patel, G.B.; Ponce, A.; Zhou, H.; Chen, W. Safety of intranasally administered archaeal lipid mucosal vaccine adjuvant and delivery (AMVAD) vaccine in mice. *Int. J. Toxicol.* **2008**, *27*, 329–339. [[CrossRef](#)] [[PubMed](#)]
30. Patel, G.B.; Sprott, G.D. Archaeobacterial ether lipid liposomes (archaeosomes) as novel vaccine and drug delivery systems. *Crit. Rev. Biotechnol.* **1999**, *19*, 317–357. [[CrossRef](#)]
31. Klasczyk, B.; Knecht, V.; Lipowsky, R.; Dimova, R. Interactions of alkali metal chlorides with phosphatidylcholine vesicles. *Langmuir* **2010**, *26*, 18951–18958. [[CrossRef](#)] [[PubMed](#)]
32. Hsueh, Y.; Chen, M.; Patty, P.J.; Code, C.; Cheng, J.; Frisken, B.J.; Zuckermann, M.; Thewalt, J. Ergosterol in POPC membranes: Physical properties and comparison with structurally similar sterols. *Biophys. J.* **2007**, *92*, 1606–1615. [[CrossRef](#)]

33. Drummond, D.C.; Meyer, O.; Hong, K.; Kirpotin, D.B.; Papahadjopoulos, D. Optimizing liposomes for delivery of chemotherapeutic agents to solid tumors. *Pharmacol. Rev.* **1999**, *51*, 691–743. [[PubMed](#)]
34. Bartlett, G.R. Phosphorus assay in column chromatography. *J. Biol. Chem.* **1959**, *234*, 466–468. [[CrossRef](#)]
35. Kanichay, R.; Boni, L.T.; Cooke, P.H.; Khan, T.K.; Chong, P.L.-G. Calcium-induced aggregation of archaeal bipolar tetraether liposomes derived from thermoacidophilic archaeon *Sulfolobus acidocaldarius*. *Archaea* **2003**, *1*, 175–183. [[CrossRef](#)]
36. Dobro, M.J.; Samson, R.Y.; Yu, Z.; McCullough, J.; Ding, H.J.; Chong, P.L.-G.; Bell, S.D.; Jensen, G.J. Electron cryotomography of ESCRT assemblies and dividing *Sulfolobus* cells suggests that spiraling filaments are involved in membrane scission. *Mol. Biol. Cell* **2013**, *24*, 2319–2327. [[CrossRef](#)] [[PubMed](#)]
37. Jameson, D.M. *Introduction to Fluorescence*; CRC Press: Boca Raton, FL, USA, 2014.
38. Pattillo, C.B.; Sari-Sarraf, F.; Nallamothu, R.; Moore, B.M.; Wood, G.C.; Kiani, M.F. Targeting of the antivascular drug combretastatin to irradiated tumors results in tumor growth delay. *Pharm. Res.* **2005**, *22*, 1117–1120. [[CrossRef](#)] [[PubMed](#)]
39. Gorner, H.; Kuhn, H.J. *Cis-trans* Photoisomerisation of Stilbenes and Stilbene-Like Molecules. *Adv. Photochem.* **2005**, *19*, 1–117.
40. Huang, J.; Buboltz, J.T.; Feigenson, G.W. Maximum solubility of cholesterol in phosphatidylcholine and phosphatidylethanolamine bilayers. *Biochim. Biophys. Acta* **1999**, *1417*, 89–100. [[CrossRef](#)]
41. Elferink, M.G.; De Wit, J.G.; Driessen, A.J.; Konings, W.N. Energy-transducing properties of primary proton pumps reconstituted into archaeal bipolar lipid vesicles. *Eur. J. Biochem.* **1993**, *214*, 917–925. [[CrossRef](#)] [[PubMed](#)]
42. Vilalta, I.; Gliozzi, A.; Prats, M. Interfacial air/water proton conduction from long distances by *Sulfolobus solfataricus* archaeal bolaform lipids. *Eur. J. Biochem.* **1996**, *240*, 181–185. [[CrossRef](#)] [[PubMed](#)]
43. Gabriel, J.L.; Chong, P.L.-G. Molecular modeling of archaeobacterial bipolar tetraether lipid membranes. *Chem. Phys. Lipids* **2000**, *105*, 193–200. [[CrossRef](#)]
44. Eisenberg, M.; Gresalfi, T.; Riccio, T.; McLaughlin, S. Adsorption of monovalent cations to bilayer membranes containing negative phospholipids. *Biochemistry* **1979**, *18*, 5213–5223. [[CrossRef](#)]
45. Matos, C.; de Castro, B.; Gameiro, P.; Lima, J.L.F.; Reis, S. Zeta-potential measurements as a tool to quantify the effect of charged drugs on the surface potential of egg phosphatidylcholine liposomes. *Langmuir* **2004**, *20*, 369–377. [[CrossRef](#)]
46. Komatsu, H.; Chong, P.L.-G. Low permeability of liposomal membranes composed of bipolar tetraether lipids from Thermoacidophilic archaeobacterium *Sulfolobus acidocaldarius*. *Biochemistry* **1998**, *37*, 107–115. [[CrossRef](#)]
47. Herbig, M.E.; Fromm, U.; Leuenerberger, J.; Krauss, U.; Beck-Sickinger, A.G.; Merkle, H.P. Bilayer interaction and localization of cell penetrating peptides with model membranes: A comparative study of a human calcitonin (hCT)-derived peptide with pVEC and pAntp(43–58). *Biochim. Biophys. Acta* **2005**, *1712*, 197–211. [[CrossRef](#)] [[PubMed](#)]
48. Ayesa, U.; Chong, P.L.-G. Polar lipid fraction E from *Sulfolobus acidocaldarius* and dipalmitoylphosphatidylcholine can form stable yet thermo-sensitive tetraether/diester hybrid archaeosomes with controlled release capability. *Int. J. Mol. Sci.* **2020**, *21*, 8388. [[CrossRef](#)]
49. Sugár, I.P. A generalization of the shell theorem. Electric potential of charged spheres and charged vesicles surrounded by electrolyte. *AIMS Biophys.* **2020**, *7*, 76–89. [[CrossRef](#)]
50. Clogston, J.D.; Patri, A.K. Zeta potential measurements. In *Characterization of Nanoparticles Intended for Drug Delivery*; McNeil, S.E., Ed.; Humana Press: New York, NY, USA, 2011; pp. 63–70.
51. Arora, A.; Raghuraman, H.; Chattopadhyay, A. Influence of cholesterol and ergosterol on membrane dynamics: A fluorescence approach. *Biochem. Biophys. Res. Commun.* **2004**, *318*, 920–926. [[CrossRef](#)] [[PubMed](#)]
52. Pottel, H.; van der Meer, W.; Herreman, W. Correlation between the order parameter and the steady-state fluorescence anisotropy of 1,6-diphenyl-1,3,5-hexatriene and an evaluation of membrane fluidity. *Biochim. Biophys. Acta* **1983**, *730*, 181–186. [[CrossRef](#)]
53. Lian, B.; Wei, H.; Pan, R.; Sun, J.; Zhang, B.; Wu, J.; Li, X.; Tian, G. Galactose modified liposomes for effective co-delivery of doxorubicin and combretastatin A4. *Int. J. Nanomed.* **2021**, *16*, 457–467. [[CrossRef](#)] [[PubMed](#)]
54. Sprott, G.D.; Dicaire, C.J.; Cote, J.; Whitfield, D.M. Adjuvant potential of archaeal synthetic glycolipid mimetics critically depends on the glyco head group structure. *Glycobiology* **2008**, *18*, 559–565. [[CrossRef](#)]
55. Šuštar, V.; Zelko, J.; Lopalco, P.; Lobasso, S.; Ota, A.; Ulrih, N.P.; Corcelli, A.; Kralj-Iglič, V. Morphology, biophysical properties and protein-mediated fusion of archaeosomes. *PLoS ONE* **2012**, *7*, e39401. [[CrossRef](#)]
56. Sprott, G.D.; Dicaire, C.J.; Gurnani, K.; Deschatelets, L.A.; Krishnan, L. Liposome adjuvants prepared from the total polar lipids of *Haloferax volcanii*, *Planococcus* spp. and *Bacillus firmus* differ in ability to elicit and sustain immune responses. *Vaccine* **2004**, *22*, 2154–2162. [[CrossRef](#)] [[PubMed](#)]
57. Müller, S.; Gruhle, K.; Meister, A.; Hause, G.; Drescher, S. Bolalipid-doped liposomes: Can bolalipids increase the integrity of liposomes exposed to gastrointestinal fluids? *Pharmaceutics* **2019**, *11*, 646. [[CrossRef](#)] [[PubMed](#)]
58. Parmentier, J.; Hofhaus, G.; Thomas, S.; Cuesta, L.C.; Gropp, F.; Schroder, R.; Hartmann, K.; Fricker, G. Improved oral bioavailability of human growth hormone by a combination of liposomes containing bio-enhancers and tetraether lipids and omeprazole. *J. Pharm. Sci.* **2014**, *103*, 3985–3993. [[CrossRef](#)] [[PubMed](#)]
59. González-Paredes, A.; Clarés-Naveros, B.; Ruiz-Martínez, M.A.; Durbán-Fornieles, J.J.; Ramos-Cormenzana, A.; Monteoliva-Sánchez, M. Delivery systems for natural antioxidant compounds: Archaeosomes and archaeosomal hydrogels characterization and release study. *Int. J. Pharm.* **2011**, *421*, 321–331. [[CrossRef](#)]

-
60. Jacobsen, A.; Jensen, S.M.; Fricker, G.; Brandl, M.; Treusch, A.H. Archaeal lipids in oral delivery of therapeutic peptides. *Eur. J. Pharm. Sci.* **2017**, *108*, 101–110. [[CrossRef](#)] [[PubMed](#)]
 61. Duse, L.; Pinnapireddy, S.R.; Strehlow, B.; Jedelska, J.; Bakowsky, U. Low level LED photodynamic therapy using curcumin loaded tetraether liposomes. *Eur. J. Pharm. Biopharm.* **2018**, *126*, 233–241. [[CrossRef](#)]